



A novel approach to charge-based non-quasi-static model of the MOS transistor valid in all modes of operation

J.M. Sallese *, A.-S. Porret

Swiss Federal Institute of Technology (EPFL), Electronics Laboratory (LEG), ELB-Ecublens, CH-1015 Lausanne, Switzerland

Received 18 March 1999; received in revised form 2 February 2000; accepted 3 February 2000

Abstract

This paper presents a new set of exact analytical expressions for the small signal analysis of the non-quasi-static operation of the MOS transistor. This model is derived from a standard charge-based description, with the help of the EKV compact model [Enz C, Krummenacher F, Vittoz E. *Analog Integ Circuits Signal Process* 1995;8:83–114.] formalism. For the first time, it gives simple expressions for all AC parameters which are valid in all operating modes, from weak to strong inversion and conduction to saturation.

The model is derived from physics and only relies on the very few basic assumptions needed for a charge-based compact model. The results are written in the form of a normalized transadmittance matrix which is expressed in terms of normalized variables (currents and frequency), so that they are independent of the process parameters. From this exact approach, simpler first- and second-order approximations, dedicated to circuit simulation tools, have been obtained. Finally, the theoretical results have been compared with measurements showing a very good agreement with measurements. © 2000 Elsevier Science Ltd. All rights reserved.

1. Introduction

It is well known that, for frequencies higher than a given device-dependant limit, the current gain of a MOS transistor is quickly degrading. This phenomenon is due to the fact that the modulation of the channel charge distribution to fast varying external potentials can no longer be considered instantaneous. Hence, neglecting these non-quasi-static (NQS) effects can result in unpredictable behavior of high-frequency circuits.

The EKV model [2], which will be used here as a framework, was initially developed [1] for low voltage applications, for which the transitions between the different modes of operation of the MOS transistor must be especially well described. Nowadays, it has evolved towards a physical charge-based description [2,3].

Despite various efforts devoted to high frequency and transient modeling of the MOS transistor, using both

numerical and analytical approaches [4–14], only incomplete sets of first-order NQS expressions were proposed for the kind of model discussed here [1,16].

The purpose of this paper is therefore to present, for the first time, an exact analytical solution of the NQS behavior of a long channel MOS transistors, based on a charge-based compact model. As, even for long-channel devices, no general NQS treatment within such a model has been presented so far, short-channel effects will not be discussed in detail. In particular, the carrier mobility will be assumed constant (see Ref. [10] for a detailed account of mobility reduction effects). However, it will be shown that, by taking into account a global DC mobility reduction, a good agreement can be achieved even for devices operated at a high overdrive gate voltage.

2. Small signal equations

In this section, the local small signal equations of the channel model, which is briefly described in Appendix A,

* Corresponding author. Tel.: +41-21-693-4601; fax: +41-21-693-3640.

E-mail address: jean-michel.sallese@epfl.ch (J.M. Sallese).

are developed. These results require no assumption on the frequency of the applied signals, so that they are still valid for the NQS operation.

2.1. Small signal approximation of the local equations

Under NQS operation, with generation–recombination mechanisms neglected, the current continuity equation [15] in the channel region can be expressed in terms of normalized time τ , normalized coordinate ξ , normalized current $i(\xi, \tau)$ and normalized channel inversion charge density $q'_1(\xi, \tau)$:

$$\frac{\partial i(\xi, \tau)}{\partial \xi} = \frac{\partial q'_1(\xi, \tau)}{\partial \tau}. \quad (1)$$

The normalized variables are related to the time t , position x along the channel, local current $I(x, t)$ and charge density $Q'_1(x, t)$ by

$$\tau = \omega_0 t \quad \text{with} \quad \omega_0 = \frac{\mu U_T}{L^2}, \quad (2)$$

$$\xi = x/L, \quad (3)$$

$$i(\xi, \tau) = I(x, t)/I_S \quad \text{with} \quad I_S = 2n\mu C'_{\text{OX}} U_T^2 W/L, \quad (4)$$

$$q'_1(\xi, \tau) = Q'_1(x, t)/Q'_{\text{SP}} \quad \text{with} \quad Q'_{\text{SP}} = 2nC'_{\text{OX}} U_T, \quad (5)$$

where W and L are the transistor width and effective length, μ is the carrier mobility, $U_T = kT/q$ is the thermodynamic voltage, n is the slope factor, and C'_{OX} is the gate oxide capacitance. The introduction of this normalization leads to considerably simpler algebraical results. (Note that a slightly different definition of I_S was adopted in Ref. [16].)

Substituting Eq. (A.4) to Eq. (1) leads to a second-order non-linear differential equation in terms of normalized charges only:

$$\frac{\partial^2}{\partial \xi^2} \left(q'_1(\xi, \tau) - q'_1(\xi, \tau)^2 \right) = \frac{\partial q'_1(\xi, \tau)}{\partial \tau}. \quad (6)$$

At this point, the small signal approximation is introduced in the form:

$$q'_1(\xi, \tau) = q'_{01}(\xi) + \delta q'_1(\xi, \tau), \quad (7)$$

$$i(\xi, \tau) = i_0 + \delta i(\xi, \tau) \quad \text{with} \quad (8)$$

$$i_0 = \frac{\partial}{\partial \xi} \left(q'_{01}(\xi) - q'_{01}(\xi)^2 \right),$$

where $q'_{01}(\xi)$ represents the static charge density at the operating point and $\delta q'_1(\xi, \tau)$ is the charge perturbation. Similarly, i_0 is the DC current, derived from Eq. (A.4), whereas $\delta i(\xi, \tau)$ is the local current fluctuation. Introducing these definitions into Eq. (6), and linearizing the result with respect to $\delta q'_1(\xi, \tau)$, leads to

$$\frac{\partial^2}{\partial \xi^2} \left[\delta q'_1(\xi, \tau) (1 - 2q'_{01}(\xi)) \right] = \frac{\partial}{\partial \tau} \delta q'_1(\xi, \tau). \quad (9)$$

And by using Eq. (8)

$$\delta i(\xi, \tau) = \frac{\partial}{\partial \xi} \left[\delta q'_1(\xi, \tau) (1 - 2q'_{01}(\xi)) \right]. \quad (10)$$

2.2. Gate and bulk currents

The normalized depletion charge density in the substrate $\delta q'_B(\xi, \tau)$ can be expressed as (see Appendix B, Eq. (B.6))

$$\delta q'_B(\xi, \tau) = -\frac{n-1}{n} \left(\delta q'_1(\xi, \tau) + \frac{1}{2n} \delta v_G(\tau) \right), \quad (11)$$

where $\delta v_G(\tau) = \delta V_G(\tau)/U_T$ is the normalized gate potential variation.

Assuming that the charge trapped in the oxide is constant with time, and by using the charge neutrality equation (B.1), the substrate $\delta I_B(t)$ and gate $\delta I_G(t)$ currents, which are assumed positive when entering the device, are simply given by

$$\delta I_B(t) = W \int_0^1 \frac{\partial Q'_B(\xi, t)}{\partial t} d\xi, \quad (12)$$

$$\begin{aligned} \delta I_G(t) &= W \int_0^1 \frac{\partial Q'_G(\xi, t)}{\partial t} d\xi \\ &= -W \int_0^1 \frac{\partial (Q'_1(\xi, t) + Q'_B(\xi, t))}{\partial t} d\xi. \end{aligned} \quad (13)$$

Then, by substituting Eq. (11) into these expressions, one gets, after normalization:

$$\begin{aligned} \delta i_B(\tau) &= -\frac{n-1}{n} \left(\int_0^1 \frac{\partial \delta q'_1(\xi, \tau)}{\partial \tau} d\xi \right) - \frac{n-1}{2n^2} \\ &\quad \times \frac{\partial \delta v_G}{\partial \tau}(\tau), \end{aligned} \quad (14)$$

$$\begin{aligned} \delta i_G(\tau) &= -\frac{1}{n} \left(\int_0^1 \frac{\partial \delta q'_1(\xi, \tau)}{\partial \tau} d\xi \right) + \frac{n-1}{2n^2} \\ &\quad \times \frac{\partial \delta v_G}{\partial \tau}(\tau). \end{aligned} \quad (15)$$

The term in parentheses can be evaluated by integrating Eq. (1) from the source ($\xi = 0$) to the drain ($\xi = 1$), so that the final result can be put in the form:

$$\begin{aligned} \delta i_B(\tau) &= -\frac{n-1}{n} (\delta i_D(\tau) - \delta i_S(\tau)) - \frac{n-1}{2n^2} \\ &\quad \times \frac{\partial \delta v_G}{\partial \tau}(\tau), \end{aligned} \quad (16)$$

$$\delta i_G(\tau) = -\frac{1}{n} (\delta i_D(\tau) - \delta i_S(\tau)) + \frac{n-1}{2n^2} \frac{\partial \delta v_G}{\partial \tau}(\tau). \quad (17)$$

It should be noted that the substrate and gate small signal currents only depend on the drain and source currents, on one side, and on the small signal gate potential variation, on the other side.

3. Harmonic analysis

In this section, the special, but most useful, case of small sinusoidal perturbations is treated. From this formulation, global transconductance equations seen from the four MOS terminals are also developed. It will therefore be assumed hereafter that the normalized potentials $\delta v_{G(D,S)}$ vary with time as

$$\delta v_{G(D,S)}(\tau) = \delta v_{G(D,S)} e^{j\Omega\tau}. \quad (18)$$

In this expression, $\delta v_{G(D,S)}$ are complex values representing, respectively, the gate, drain and source small signal amplitude, $\Omega = \omega/\omega_0$ is the normalized angular frequency and j is the imaginary number $\sqrt{-1}$. Similarly, the inversion charge expression becomes

$$\delta q'_1(\xi, \tau) = \delta q'_1(\xi, \Omega) e^{j\Omega\tau}. \quad (19)$$

Substituting Eq. (19) into Eq. (9) and using the expression (A.6) for $q'_0(\xi)$ leads to

$$\begin{aligned} \frac{\partial^2}{\partial \xi^2} \left[\delta q'_1(\xi, \Omega) \sqrt{1 + 4(i_f(1 - \xi) + \xi i_r)} \right] \\ = j\Omega \delta q'_1(\xi, \Omega). \end{aligned} \quad (20)$$

After some calculations, and provided that the DC current is not null ($i_f \neq i_r$), the general solution of the latter equation can be written as a linear combination of Bessel functions of order the $\frac{2}{3}$ and $-\frac{2}{3}$:

$$\delta q'_1(\xi, \Omega) = C_1 J_{2/3}[F(\xi, \Omega)] + C_2 J_{-2/3}[F(\xi, \Omega)], \quad (21)$$

where C_1 and C_2 depend on the boundary conditions, and the auxiliary function $F(\xi, \Omega)$ was introduced:

$$F(\xi, \Omega) = e^{-j(\pi/4)} \sqrt{\Omega} \frac{[1 + 4(i_f(1 - \xi) + i_r \xi)]^{3/4}}{3(i_f - i_r)}. \quad (22)$$

Appendix C describes how to calculate C_1 and C_2 from the value of the applied potentials, whereas the special case corresponding to $i_f = i_r$ is treated separately in Appendix D.

Finally, substituting Eq. (21) into Eq. (10) leads to the expression of the NQS small signal channel current as a function of the normalized coordinate ξ :

$$\begin{aligned} \delta i(\xi, \Omega) = e^{j(3\pi/4)} \sqrt{\Omega} [1 + 4(i_f(1 - \xi) + i_r \xi)]^{1/4} \\ \times (C_1 J_{-1/3}[F(\xi, \Omega)] - C_2 J_{1/3}[F(\xi, \Omega)]). \end{aligned} \quad (23)$$

And then, by using Eqs. (16) and (17), the currents through the four terminals follow:

$$\begin{aligned} \delta i_S(\Omega) &= \delta i(0, \Omega), \\ \delta i_D(\Omega) &= \delta i(1, \Omega), \\ \delta i_G(\Omega) &= \frac{\delta i(0, \Omega) - \delta i(1, \Omega)}{n} + j\Omega \frac{n-1}{2n^2} \delta v_G, \\ \delta i_B(\Omega) &= \frac{n-1}{n} (\delta i(0, \Omega) - \delta i(1, \Omega)) - j\Omega \frac{n-1}{2n^2} \delta v_G. \end{aligned} \quad (24a-d)$$

By convention, all currents entering the device are considered positive, except at the source.

4. Normalized transadmittances

The normalized transadmittances $y_{\alpha\beta}$ are defined as the ratio of the small signal normalized current δi_α flowing through terminal α , and of the normalized voltage δv_β at node β :

$$y_{\alpha\beta} = Y_{\alpha\beta} \frac{U_T}{I_S} = \left. \frac{\delta i_\alpha}{\delta v_\beta} \right|_{\delta v_{z \neq \beta} = 0}, \quad (25)$$

where $Y_{\alpha\beta}$ is the usual, unnormalized, transadmittance. Some general properties linking the different transadmittances may be found in Appendix E.

For an implementation in a simulating tool, the general transadmittance expressions, in terms of Bessel functions with complex arguments, are not efficient as their evaluation is time consuming. Hence, simpler first- and second-order developments, in power series of Ω , can be derived using a polynomial expansion of the Bessel functions. The general form of the second order normalized transadmittances becomes

$$y_{\alpha\beta}(\Omega) = \frac{N_0^{\alpha\beta} + N_1^{\alpha\beta}(j\Omega) + N_2^{\alpha\beta}(j\Omega)^2}{1 + D_1(j\Omega) + D_2(j\Omega)^2}. \quad (26)$$

Introducing the intermediate variables χ_f and χ_r :

$$\chi_{f(r)} = \sqrt{\frac{1}{4} + i_{f(r)}}, \quad (27)$$

and after some rearrangement, the coefficients of Eq. (26) can be expressed in terms of χ_f and χ_r only, as given in Table 1.

Going a step further, $y_{\alpha\beta}$ can be limited to its first order development, reducing to

$$Y_{\alpha\beta} = g_{\alpha\beta} + j\omega C_{\alpha\beta}, \quad (28)$$

where $g_{\alpha\beta}$ and $C_{\alpha\beta}$ represent the transconductance and transcapacitance between nodes α and β . They can be either positive or negative, depending on the adopted current convention.

The results of these calculations, again expressed as functions of χ_f and χ_r only, are listed in Table 2. Obviously, such expressions for $Y_{\alpha\beta}$ can only be used for

Table 1
Second-order normalized transadmittance coefficients used in Eq. (26)^a

Variable	Expression
$N_0^{\text{DG}} = N_0^{\text{SG}}$	$(\chi_f - \chi_r)/n$
$N_1^{\text{DG}}, (-N_1^{\text{SG}})$	$-\frac{1}{6n} \left((2\chi_{r(f)-1})(2\chi_{f(f)} + \chi_{r(f)}) / (\chi_f + \chi_r)^2 \right)$
$N_2^{\text{DG}}, (-N_2^{\text{SG}})$	$-\frac{1}{180n} \left((5\chi_{f(f)}^2 + 8\chi_f\chi_r + 2\chi_{r(f)}^2)(2\chi_{r(f)} - 1) / (\chi_f + \chi_r)^4 \right)$
N_0^{DS}	$\frac{1}{2} - \chi_f$
N_0^{SD}	$\chi_r - \frac{1}{2}$
$N_1^{\text{DS}} = N_1^{\text{SD}}$	0
$N_2^{\text{DS}} = N_2^{\text{SD}}$	0
D_1	$\frac{2}{15} \left((\chi_f^2 + 3\chi_f\chi_r + \chi_r^2) / (\chi_f + \chi_r)^3 \right)$
D_2	$\frac{1}{180} \left((\chi_f^2 + 4\chi_f\chi_r + \chi_r^2) / (\chi_f + \chi_r)^4 \right)$

^a Variables in parentheses correspond to indices in parentheses in the expressions.

“low” frequencies where distributed effects are almost negligible.

Only six independent real parameters (four transcapacitances and two transconductances) are needed to fully describe the low frequency, small signal, behavior of the intrinsic MOS transistor. Note also that the intrinsic transcapacitances are non-reciprocal but satisfy the charge conservation condition.

5. Comparison with measurements

5.1. MOS operated in saturation mode

In order to validate the model, experimental data taken from the literature have been used. These high frequency measurements were performed on PMOS transistors with 10 and 30 μm channel length and have been published by Klaassen et al. [11, Fig. 10]. Although parameters as the threshold voltage V_{T0} may slightly depend on the compact model used for their extraction (Philips MOS Model 9 in Ref. [11] and EKV in this paper), the original values have been kept: $V_{T0} = 1.11$ V; hole mobility $\mu_p = 15.5 \times 10^{-3}$ m^2/Vs ; $C'_{\text{OX}} = 2.3$ E-3 F m^{-2} . For this experiment, the gate and drain

voltages were fixed at 4 V, leading to normalized forward and reverse currents of 2200 and 0, respectively. The mobility reduction due to the vertical field was extracted from the DC transconductance.

The normalized y_{DG} data are plotted in Fig. 1a (magnitude) and b (phase). The set of curves (a), in both figures, depicts the normalized transconductances for the three channel lengths, in saturation mode. The corresponding theoretical characteristics, calculated in terms of Bessel functions, are also shown (note that, in Fig. 1a, $n y_{\text{DG}}$ is plotted instead of y_{DG}). A very good agreement between theory and experiment can be observed, both for the magnitude and phase characteristics, even for submicrometer devices. It can be noted that the phase shift appears well before the decrease in the magnitude of y_{DG} . This supports the accuracy of the model, as phase shift is difficult to predict precisely, especially over a large range of variation, as in the present case. Above a normalized frequency of about 2000, the magnitude and phase starts to increase. This effect can be attributed to some extrinsic capacitance, which are neglected in the model.

Curves labeled (b)–(e) show the evolution of the magnitude and phase characteristics of the model in saturation mode, from weak to strong inversion. As can

Table 2
First-order AC parameters, with $C_{\text{OX}} = C'_{\text{OX}} W L^a$

Variable	Expression
$g_{\text{DS}} U_T / I_S (-g_{\text{SD}} U_T / I_S)$	$\frac{1}{2} - \chi_{f(f)}$
$g_{\text{DG}} = g_{\text{SG}}$	$-(g_{\text{DS}} + g_{\text{SD}})/n$
$C_{\text{DG}}/C_{\text{OX}} (-C_{\text{SG}}/C_{\text{OX}})$	$-\frac{1}{15} \left((4\chi_{f(f)}^3 + 6\chi_{r(f)}^3 + 28\chi_{f(f)}^2\chi_{r(f)} - 10\chi_{r(f)}^2 - 15\chi_f\chi_r + 22\chi_{r(f)}\chi_{r(f)}^2 - 5\chi_{r(f)}^2) / (\chi_f + \chi_r)^3 \right)$
$C_{\text{DS}}/C_{\text{OX}} (-C_{\text{SD}}/C_{\text{OX}})$	$\frac{2n}{15} (2\chi_{f(f)} - 1) (\chi_f^2 + \chi_r^2 + 3\chi_f\chi_r) / (\chi_f + \chi_r)^3$

^a The other transcapacitances can be obtained by using Eqs. (E.2) and (E.3). Variables in parentheses correspond to indices in parentheses in the expressions.

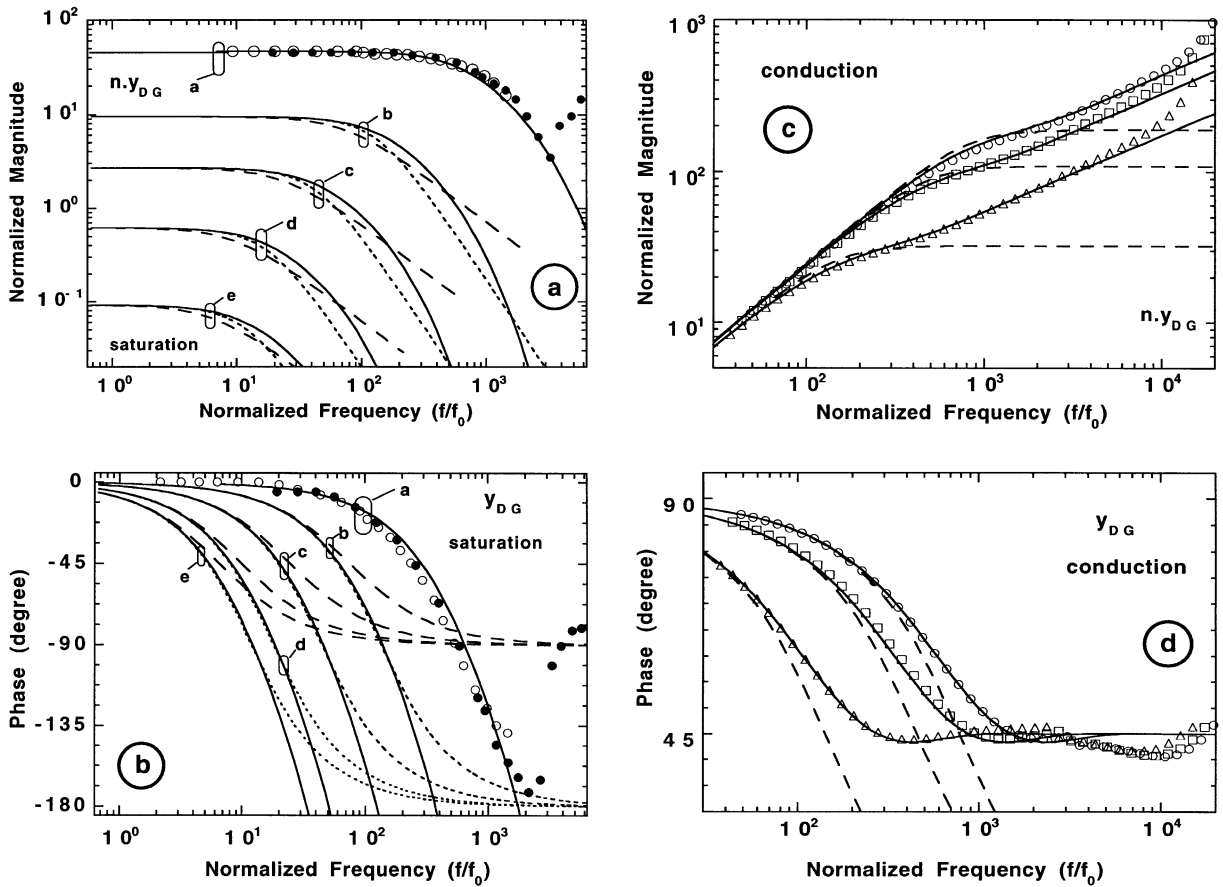


Fig. 1. Plots a and b: Comparison between the exact (—), the first-order (- - -) and the second-order (· · ·) expressions of $n y_{DG}$ magnitude (plot a) and phase (plot b) versus the normalized frequency in saturation, from weak to strong inversion (curve a: $i_f = 10^3$; b: $i_f = 10^2$; c: $i_f = 1$; d: $i_f = 10^{-1}$). Solid circles and open circles correspond to reported data for MOS transistors of 30 and 10 μm channel length, respectively. Plots c and d: Comparison between theoretical (—) and measured data of the magnitude (plot c) and phase (plot d) of y_{DG} (normalized) at $V_{DS} = 0$ for different levels of inversion (\circ : $i_f = 1470$; \square : $i_f = 500$; \triangle : $i_f = 50$). Dashed lines represent the second-order approximation.

be observed, the NQS effects are shifted towards higher frequencies when the inversion factor is increased. This shift is proportional to $\sqrt{i_f}$ in strong inversion mode and gets constant in weak inversion. The first- and second-order approximations of the transconductances are also shown. As expected, the accuracy of the second-order expressions is far better than the first-order one and appears to be sufficient for most practical applications. The agreement is fairly good for phase lags lower than 110°. On the contrary, the accuracy of the first-order expansion already degrades rapidly for phase shifts exceeding 30°.

5.2. MOS operated in conduction mode

This section discusses the evolution of the Y_{DG} transconductance, in the conduction mode, for $V_{DS} = 0$, cor-

responding to the use of the transistor as a MOS capacitor. Measurements have been realized on NMOS devices of size $W \times L = 100 \times 300 \mu\text{m}$, integrated in a 0.35 μm process. The corresponding EKV parameters were: $V_{T0} = 0.509$; $\Gamma = 0.564$; $\Phi = 0.881$; $E_0 = 98 \text{ E-6}$; $K_p = 211 \text{ E-6}$ [2]. The use of such long and large structures allowed to neglect extrinsic effects such as overlap capacitance. The measurements were performed under different gate bias conditions with an HP4285 LCR-meter.

Fig. 1c and d shows the module and phase of the normalized transconductance y_{DG} under various levels of inversion, both for theoretical and experimental data, and without any parameter fitting. The agreement between the theory and measurements is very good. Again, for very high frequencies ($\Omega > 3000$), extrinsic elements, mostly due to the measurement setup itself, gradually degrades accuracy.

At low frequencies, relative to NQS effects, the y_{DG} frequency dependence is very close to a capacitor, the amplitude varying with a 20 dB per decade slope. In the same way, the phase shift tends towards 90° . As the frequency increases, the discrepancy with the capacitance behavior rapidly grows. The y_{DG} magnitude starts to vary with a 10 dB per decade slope, which is confirmed by the stabilization of the phase shift around 45° , indicating that the channel mostly operates like an RC transmission line. It can be noted that even the bump in the phase curves, before saturation at 45° , is correctly predicted by the model. Unfortunately, these plots also show that even the second-order approximation is not able to model a distributed elements behavior with a sufficient accuracy, at least for phase shifts lower than 60° .

6. Conclusion

For the first time, an exact analytical by small signal NQS model of the MOS transistor, which is valid in all modes of operation and from DC to high frequencies, was presented. This is derived from a general charge-based approach and uses the framework of the EKV model. It has been demonstrated that only four independent transadmittances are needed to fully characterize the small signal operation of the device. All quantities in the model are expressed in terms of normalized variables, which are independent of the process parameters.

Comparison with published and measured data showed a very good agreement with the model in all the regions of operation, without introducing any fitting parameter.

Finally, first- and second-order approximation of the analytical solutions, aimed at simulation tools, were presented and their limit of application discussed.

Acknowledgements

We would like to thank Amy Ils, Matthias Bucher, Christian Enz, François Krummenacher and Wladek Grabinski for helpful assistance and discussion. We would also like to express our appreciation to Professor Pierre Fazan for allowing us to complete this work.

Appendix A. Basic local equations and DC model

According to the EKV model, all voltages are referenced to the bulk, as a consequence of the intrinsic device symmetry. Among the concepts required by this formulation, the pinch off voltage V_p plays a major role.

This voltage expresses the effect of the gate voltage V_G on the channel and is given by

$$V_p = \frac{V_G - V_{T0}}{n} \quad \text{with } n = 1 + \frac{\gamma}{2\sqrt{V_p + \Psi_0}}, \quad (\text{A.1})$$

where V_{T0} is the threshold voltage, n the slope factor, and γ the body effect coefficient. Ψ_0 is usually approximated by $2\phi_F +$ several U_T , where ϕ_F is the well Fermi potential [1].

Assuming a constant gate potential, the inversion charge density Q'_I can be expressed in terms of the surface potential, in differential form [17]:

$$dQ'_I = nC'_{OX} d\Psi_S, \quad (\text{A.2})$$

where Ψ_S is the surface potential, and Q'_I is the channel charge density per unit area. Then, the channel current (including diffusion and drift currents) is simply given by

$$I(x, t) = W\mu \frac{\partial}{\partial x} \left(-\frac{Q'_I(x, t)^2}{2nC'_{OX}} + U_T Q'_I(x, t) \right). \quad (\text{A.3})$$

Eq. (A.3) can be expressed in terms of normalized current $i(\xi, t)$, charge $q'_I(\xi, t)$ and coordinate ξ (see Eqs. (3)–(5)), leading to

$$i(\xi, t) = \frac{\partial}{\partial \xi} \left(q'_I(\xi, t) - q'_I(\xi, t)^2 \right). \quad (\text{A.4})$$

Integrating from the source ($\xi = 0$) to the drain ($\xi = 1$), the normalized channel current can be split into forward i_f and reverse i_r contributions, which are related to the normalized source and drain inversion charges q'_S and q'_D [1,18]:

$$i = i_f - i_r, \quad \text{with } i_{f(r)} = q'^2_{S(D)} - q'_{S(D)}. \quad (\text{A.5})$$

Note that saturation corresponds to the case where $i_f \gg i_r$; otherwise, the MOS is assumed in conduction mode. Strong, weak and moderate inversions correspond, respectively, to i_f much greater, much lower or close to 1.

Integrating Eq. (A.3) and using Eq. (A.5), while noting that the DC current $i(\xi, t)$ is constant along the channel, leads to the expression of the inversion charge density as a function of the coordinate ξ , which will be required for the NQS derivation:

$$q'_I(\xi) = \frac{1}{2} - \sqrt{\frac{1}{4} + i_f(1 - \xi) + i_r \xi}. \quad (\text{A.6})$$

Introducing the normalized drain and source voltages $v_{D(S)} = V_{D(S)}/U_T$ and expressing the drain and source transconductances [1] in normalized units gives

$$\left. \frac{\partial i}{\partial v_{D(S)}} \right|_{V_G, V_{S(D)}} = -(+) q'_{D(S)}. \quad (\text{A.7})$$

Then, substituting Eq. (A.7) into Eq. (A.5) and supposing that the channel charges at the drain (source) are

not functions of the source (drain) potential (this assumption does not hold when velocity saturation effects occurs in short channels):

$$\frac{\partial}{\partial v_{S(D)}} \left(q'_{S(D)^2} - q'_{S(D)} \right) \Big|_{v_G} = q'_{S(D)}. \quad (\text{A.8})$$

By integration, and reminding that in strong inversion $q'_{S(D)} = (v_{S(D)} - v_P)/2$ [1]:

$$\ln \left(-q'_{S(D)} \right) - 2q'_{S(D)} = v_P - v_{S(D)}. \quad (\text{A.9})$$

Finally, combining Eqs. (A.9) and (A.5) allows us to calculate the DC normalized currents. (Note that this approach does not require an additional variable, i_P , which cannot be calculated, as in Ref. [16]). For more information, a complete methodology for EKV parameter extraction as well as analytical expressions implemented in CAD tools are given in Refs. [2,19].

Appendix B. Bulk depletion charge

In this appendix, the expression of the bulk depletion charge Q'_B will be derived. It will be assumed that Q'_B responds immediately to surface potential variations. The global charge neutrality equation of the MOS transistor can be written as

$$Q'_G(t) + Q'_{OX} + \int_0^1 Q'_1(\xi, t) d\xi + \int_0^1 Q'_B(\xi, t) d\xi = 0, \quad (\text{B.1})$$

where Q'_{OX} is the total fixed charges in the oxide (supposed to be constant with time and voltages). $Q'_1(\xi, t)$ and $Q'_B(\xi, t)$ are related to the gate and surface potentials by [15]

$$Q'_1(\xi, t) = -C'_{OX} \left(V_G(t) - V_{FB} - \Psi_S(\xi, t) - \gamma \sqrt{\Psi_S(\xi, t)} \right), \quad (\text{B.2})$$

$$Q'_B(\xi, t) = -C'_{OX} \gamma \sqrt{\Psi_S(\xi, t)}, \quad (\text{B.3})$$

where V_{FB} is the flat band voltage. Differentiating Eqs. (B.2) and (B.3) around $\Psi_S(\xi, t) = 2\phi_F(\xi, t) + V_P(t)$ [17] and allowing for gate voltage variation results in

$$\delta Q'_1(\xi, t) = C'_{OX} (n\delta\Psi_S(\xi, t) - \delta V_G(t)), \quad (\text{B.4})$$

$$\delta Q'_B(\xi, t) = -C'_{OX} (n - 1)\delta\Psi_S(\xi, t). \quad (\text{B.5})$$

Finally, after substitution,

$$\delta Q'_B(\xi, t) = -\frac{n-1}{n} \left(\delta Q'_1(\xi, t) + \frac{C'_{OX}}{2n} \delta V_G(t) \right). \quad (\text{B.6})$$

Appendix C. Boundary conditions

To obtain a complete solution to the problem, C_1 and C_2 coefficients in Eq. (23) have to be determined using appropriate boundary conditions. Supposing that the inversion charge densities at both channel ends are at equilibrium with the applied potentials, i.e. that the densities respond instantaneously to the applied external bias, Eq. (A.9) remains valid at any time at these two points. Differentiating the latter equation with respect to the external voltages leads then to the following conditions:

$$\delta q'_{S(D)} = \frac{1}{2} \left(\frac{\delta v_G}{n} - \delta v_{S(D)} \right) \left(\frac{1}{\sqrt{1+4i_f(t)}} - 1 \right). \quad (\text{C.1})$$

Thus, the coefficients C_1 and C_2 can be determined by evaluating Eq. (21) at the source and drain and comparing with (C.1):

$$C_1 = \frac{\delta q'_S J_{-2/3}[F(1, \Omega)] - \delta q'_D J_{-2/3}[F(0, \Omega)]}{J_{-2/3}[F(1, \Omega)] J_{2/3}[F(0, \Omega)] - J_{-2/3}[F(0, \Omega)] J_{2/3}[F(1, \Omega)]},$$

$$C_2 = \frac{\delta q'_D J_{2/3}[F(0, \Omega)] - \delta q'_S J_{2/3}[F(1, \Omega)]}{J_{-2/3}[F(1, \Omega)] J_{2/3}[F(0, \Omega)] - J_{-2/3}[F(0, \Omega)] J_{2/3}[F(1, \Omega)]}. \quad (\text{C.2a, b})$$

Appendix D. Special “resistive” case, $V_D = V_S$

When $i_f = i_r$ and $i = 0$, the equations developed in the body of the paper are not directly applicable. It can be shown that, in this case, the general solution is a linear combination of exponential functions:

$$\delta q'_1(\xi, \Omega) = C_1 e^{\lambda \xi} + C_2 e^{-\lambda \xi} \quad \text{with}$$

$$\lambda = \frac{e^{j(\pi/4)} \sqrt{\Omega}}{(1+4i_f)^{1/4}}, \quad (\text{D.1})$$

$$\delta i(\xi, \Omega) = \sqrt{1+4i_f} (C_1 \lambda e^{\lambda \xi} - C_2 \lambda e^{-\lambda \xi}). \quad (\text{D.2})$$

C_1 and C_2 coefficients are given by

$$C_1 = \frac{\delta q'_D - \delta q'_S e^{-\lambda}}{e^\lambda - e^{-\lambda}} \quad \text{and} \quad C_2 = \frac{-\delta q'_D + \delta q'_S e^\lambda}{e^\lambda - e^{-\lambda}}. \quad (\text{D.3})$$

A comparison (not shown here) between exact and approximated expressions for the transadmittances carried out for $i_f = i_r$ showed that the first and second order expressions reported in Tables 1 and 2 are still valid for this particular case.

Appendix E. General transadmittances properties

In our analysis, as the bulk is the voltage reference, a variation δv of the bulk potential will have the same

effect as a simultaneous variation $-\delta v$ on the gate, source and drain nodes. In terms of transadmittances, this can be written as

$$y_{\alpha B}(\Omega) = -y_{\alpha G}(\Omega) - y_{\alpha S}(\Omega) - y_{\alpha D}(\Omega), \quad (\text{E.1})$$

where α holds for drain, source, gate or bulk terminal. From Eq. (C.1), the effect of a gate potential variation δv_G is identical to a simultaneous change of the drain and source potential by $-\delta v_G/n$. This symmetry gives, in terms of transconductances:

$$\begin{aligned} y_{SS}(\Omega) &= -ny_{SG}(\Omega) - y_{SD}(\Omega), \\ y_{DD}(\Omega) &= -ny_{DG}(\Omega) - y_{DS}(\Omega). \end{aligned} \quad (\text{E.2a, b})$$

Then, by combining Eqs. (24c,d) with Eqs. (E.1) and (E.2), the other relations can easily be obtained:

$$\begin{aligned} y_{GD}(\Omega) &= \frac{y_{SD}(\Omega) + y_{DS}(\Omega)}{n} + y_{DG}(\Omega), \\ y_{GS}(\Omega) &= -\frac{y_{SD}(\Omega) + y_{DS}(\Omega)}{n} - y_{SG}(\Omega), \\ y_{BD(S)}(\Omega) &= (n-1)y_{GD(S)}(\Omega), \\ y_{BG}(\Omega) &= \frac{n-1}{n}(y_{SG}(\Omega) - y_{DG}(\Omega)) - j\Omega \frac{n-1}{2n^2}, \\ y_{BB}(\Omega) &= -y_{BG}(\Omega) - y_{BS}(\Omega) - y_{BD}(\Omega), \\ y_{GG}(\Omega) &= y_{SG}(\Omega) - y_{DG}(\Omega) - y_{BG}(\Omega), \\ y_{D(S)B}(\Omega) &= (n-1)y_{D(S)G}(\Omega), \\ y_{GB}(\Omega) &= y_{BG}(\Omega). \end{aligned} \quad (\text{E.3a-h})$$

Thus, according to the above analysis and knowing the slope factor n , only four independent normalized transadmittances, namely $y_{SG}(\Omega)$, $y_{DG}(\Omega)$, $y_{DS}(\Omega)$ and $y_{SD}(\Omega)$, are needed to describe completely the 16 terms of the normalized matrix impedance.

References

- [1] Enz C, Krummenacher F, Vittoz E. An analytical MOS transistor model valid in all regions of operation and dedicated to low-voltage and low-power applications. *Analog Integ Circuits Signal Proc* 1995;8:83–114.
- [2] Bucher M, Lallement C, Enz C, Théodoloz F, Krummenacher F. The EPFL-EKV MOSFET model equations for simulation, model version 2.6. Technical Report, Electronic Laboratories, Swiss Federal Institute of Technology EPFL, Lausanne, Switzerland, 1997, The complete description of the model can be found on the WEB at: legwww.epfl.ch/ekv.
- [3] Bucher M, Lallement C, Enz C, Théodoloz F, Krummenacher F. Scalable GM/I based MOSFET model. *Proceedings of the International Semiconductor Device Research Symposium, Charlottesville, VA, 1997*. p. 615–8.
- [4] Bagheri M, Tsividis Y. A small signal dc-to-high-frequency nonquasistatic model for the four-terminal MOSFET valid in all regions of operation. *IEEE Trans Electron Dev* 1985;ED-32(11):2383–91.
- [5] Mancini P, Turchetti C, Masetti G. A non-quasi-static analysis of the transient behavior of the long-channel MOST valid in all regions of operation. *IEEE Trans Electron Dev* 1987;ED-34(2):325–34.
- [6] Vandelloo PJV, Sansen WMC. Modeling of the MOS transistor for high frequency analog design. *IEEE Trans Comp-Aided Design* 1989;8(7):713–23.
- [7] Park H-J, Ko PK, Hu C. A charge conserving non-quasi-static (NQS) MOSFET model for SPICE transient analysis. *IEEE Trans Comp-Aided Design* 1991;10(5):629–42.
- [8] Park H-J, Ko PK, Hu C. A non-quasi-static MOSFET model for SPICE-AC analysis. *IEEE Trans Comp-Aided Design* 1992;11(10):1247–57.
- [9] Vanoppen RRJ, Geelen JAM, Klaassen DBM. The high frequency analogue performance of MOSFETs. *Proceedings of the International Electron Device Meeting Conference, 1994*. p. 173–6.
- [10] Smedes T, Klaassen FM. An analytical model for the non-quasi-static small-signal behavior of submicron MOSFETs. *Solid-State Electron* 1995;38(1):121–30.
- [11] Klaassen DBM, Nauta B, Vanoppen RRJ. RF modelling of MOSFETs. *Proceedings of the workshop on Advances in Analog Circuit Design, Lausanne, Switzerland, 1996*. p. 1–22.
- [12] Liu W, Gharpurey R, Chang MC, Erdogan U, Aggarwal R, Mattia JP. RF MOSFET modeling accounting for distributed substrate and channel resistances with emphasis on the BSIM3v3 SPICE model. *Proceedings of the International Electron Device Meeting Conference, 1997*. p. 173–6.
- [13] Klaassen DBM, van Langevelde R, Scholten AJ, Tiemeijer LF. Challenges in compact modelling of future RF CMOS. *Proceedings of the 29th European Solid-State Device Research Conference ESSDERC, Leuven, Belgium, 1999*. p. 95–102.
- [14] Tiemeijer LF, de Vreede PWH, Scholten AJ, Klaassen DBM. MOS model nine based non-quasi-static small-signal model for RF circuit design. *Proceedings of the 29th European Solid-State Device Research Conference ESSDERC, Leuven, Belgium, 1999*. p. 652–5.
- [15] Tsividis YP. *Operation and modeling of the MOS transistor*. New York: McGraw-Hill, 1999.
- [16] Cunha AIA, Schneider MC, Galup-Montoro C. An MOS transistor model for analog circuit design. *IEEE Solid-State Circ* 1998;33(10):1510–9.
- [17] Cunha AIA, Schneider MC, Galup-Montoro C. An explicit physical model for the long-channel MOS transistor including small-signal parameters. *Solid-State Electron* 1995;38(11):1945–52.
- [18] Cunha AIA, Gouveia-Filho OC, Schneider MC, Galup-Montoro C. A current based model for the MOS transistor. *Proc IEEE Int Symp Circ Syst* 1997;3:1608–11.
- [19] Bucher M, Lallement C, Enz C. An efficient parameter extraction methodology for the EKV MOST model. *Proc IEEE Int Conf Test Struct* 1996;9:145–50.